ResearchGate

See discussions, stats, and author profiles for this publication at: https://www.researchgate.net/publication/23157303

Thermodynamics of water intrusion in nanoporous hydrophobic solids

Article *in* Physical Chemistry Chemical Physics · September 2008

DOI: 10.1039/b807471b · Source: PubMed

CITATIONS
114

READS
483

7 authors, including:

Fabien Cailliez
Université Paris-Saclay
39 PUBLICATIONS **1,285** CITATIONS
SEE PROFILE

Isabelle Demachy
Université Paris-Saclay
75 PUBLICATIONS **1,848** CITATIONS
SEE PROFILE

Joël Patarin
Université de Haute-Alsace
413 PUBLICATIONS **12,250** CITATIONS
SEE PROFILE

All content following this page was uploaded by Fabien Cailliez on 01 June 2014.

The user has requested enhancement of the downloaded file.

PCCP

Physical Chemistry Chemical Physics

www.rsc.org/pccp

Volume 10 | Number 32 | 28 August 2008 | Pages 4661–5016

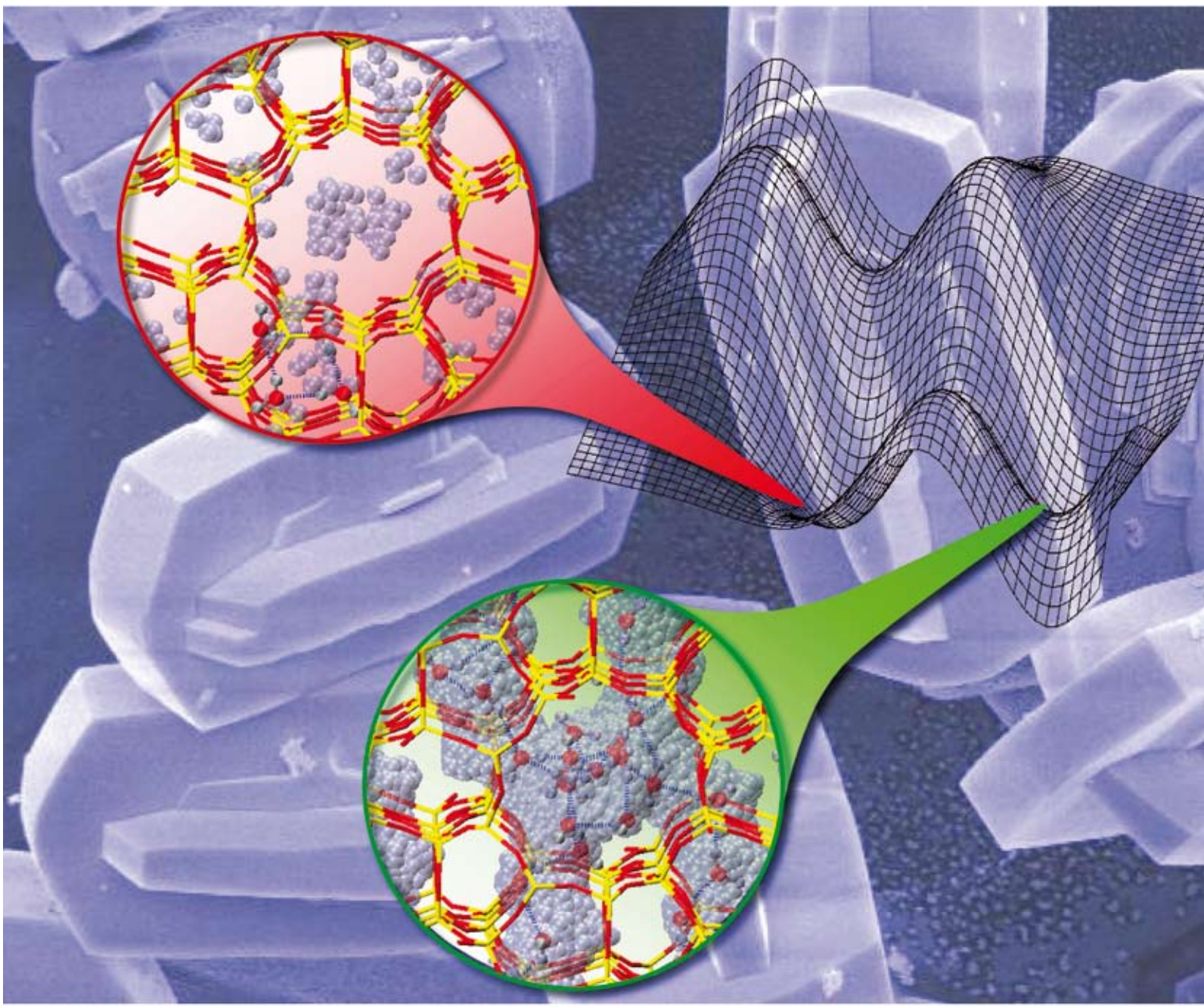

ISSN 1463-9076

THEMED ISSUE
Water at Interfaces

COVER ARTICLE
Fuchs *et al.*
Thermodynamics of water intrusion in nanoporous hydrophobic solids

HOT ARTICLE
Vendrell and Meyer
A proton between two waters: insight from full-dimensional quantum-dynamics simulations of the $[H_2O–H–OH_2]^+$ cluster

1463-9076 (2008) 10:32;1-#

Thermodynamics of water intrusion in nanoporous hydrophobic solids

Fabien Cailliez,[a] Mickael Trzpit,[b] Michel Soulard,[b] Isabelle Demachy,[c] Anne Boutin,[c] Joël Patarin[b] and Alain H. Fuchs*[a]

Received 2nd May 2008, Accepted 24th June 2008
First published as an Advance Article on the web 9th July 2008
DOI: 10.1039/b807471b

We report a joint experimental and molecular simulation study of water intrusion in silicalite-1 and ferrerite zeolites. The main conclusion of this study is that water condensation takes place through a genuine first-order phase transition, provided that the interconnected pores structure is 3-dimensional. In the extreme confinement situation (ferrierite zeolite), condensation takes place through a continuous transition, which is explained by a shift of both the first-order transition line and the critical point with increasing confinement. The present findings are at odds with the common belief that conventional phase transitions cannot take place in microporous solids such as zeolites. The most important features of the intrusion/extrusion process can be understood in terms of equilibrium thermodynamics considerations. We believe that these findings are very general for hydrophobic solids, *i.e.* for both nonwetting as well as wetting water–solid interface systems.

1. Introduction

The concept of *hydrophobicity* was first used in aqueous solution thermodynamics in order to explain the solubility of small non polar species in water.[1] Such species can be accommodated in small quantities in liquid water without much perturbation of its hydrogen-bonded (HB) network. As the species gets larger, it becomes impossible to maintain the integrity of the HB network. For a large enough solute, it has been suggested that this could lead to the formation of a very thin layer of vapour separating the non polar surface from the liquid (an effect called "surface dewetting").[2,3] Lum *et al.*[4] have argued that this qualitative change in behaviour from a "small" to a "large" solute could be characterized by a crossover length of the order of 1 nm. A recent large-scale simulation has confirmed this theory.[5] A comprehensive review on this subject, and its link with the role of water in biology, was provided by P. Ball very recently.[6]

The term hydrophobic is somewhat misleading since it literally means "water repelling". Indeed, in several theoretical studies, hydrophobic species were simply modeled as purely repulsive.[4,7] In real life, the water–hydrophobe interaction is attractive but less than the mutual water–water attraction. We shall use here this very simple and straightforward definition of a hydrophobic species, based on the comparison between the hydrophobe–water and the water–water interaction potential energy.

More recently, the notion of *surface hydrophobicity* was used.[8–10] It should be understood as a simple extension of the concept of hydrophobicity for large solutes described above. When a water molecule approaches a purely graphitic carbon surface, for instance, it experiences a weaker potential interaction energy than in the bulk liquid state, which is due to the lack of HB between water and carbon atoms. A similar situation is encountered when water is interacting with a protein surface made of nonpolar residues.

The behaviour of water confined to spaces of nanoscopic dimensions is an important issue in many areas of science and technology.[11,12] The special situations in which the confining surfaces are hydrophobic have attracted a lot of interest in the past decade. Understanding the changes in water properties due to interactions with a hydrophobic substrate is relevant to such problems as selective adsorption using activated carbons or all-silica zeolites[13,14] (waste water treatment for instance). Similar questions arise when considering the issue of confined water in biological channels[15,16] and protein cavities.[17,18] We shall use for the rest of this article the term *hydrophobic solid* to depict a porous solid, the internal surface of which is hydrophobic.

Porous carbon materials are archetypical hydrophobic solids. They have been extensively studied for fundamental as well as practical reasons.[19] Adsorption studies of water vapour have been reported for several types of activated carbons.[20–27] A weak adsorption was always observed in the low-pressure range of the adsorption isotherms, on account of the fact that the water–carbon dispersion interaction is approximately an order of magnitude weaker than the mutual water–water attraction.[28] Adsorption remains low up to a relative pressure P/P_0 of 0.4 or more (where P_0 is the bulk saturation vapour pressure). This is followed by either a gradual[22,23] or a sudden[24,26] water uptake, depending on the type of activated carbon sample, taking place at a relative pressure near saturation (for instance $P/P_0 \sim 0.8$ in the case of the "P20Ar" sample studied by Kaneko and coworkers[24]). This water condensation phenomenon is usually accompanied by a hysteresis loop (the desorption transition taking place at a lower

[a] *Ecole nationale supérieure de chimie de Paris (Chimie ParisTech) and Université Pierre et Marie Curie-Paris 6, 75005, France. E-mail: alain.fuchs@enscp.fr*
[b] *Ecole nationale supérieure de chimie de Mulhouse, Université de Haute Alsace and CNRS, 68093 Mulhouse, France*
[c] *Université Paris-Sud and CNRS, 91405 Orsay, France*

relative pressure value than in the adsorption branch). The experimental water condensation pressure depends on the type of activated carbon sample, in a way that is not well understood.[23] It has been suggested for a long time that the surface chemical species present in activated carbon materials (typically oxygenated polar groups) play a crucial role on the observed water condensation process. According to the Dubinin-Serpinsky model,[25] water condenses around these surface defects and form clusters, the size of which gradually grows upon pressure increase, until a full condensation takes place. The condensation process is also known to depend on the pore size, but this was again thought to be "masked by the influence of the surface groups".[23]

In an attempt to discriminate between the generic properties of pure carbon nanopores and the real-life defective materials, several groups have undertaken a molecular simulation study of a slit-shaped graphitic pore,[29–33] which is believed to provide a fair local representation of activated carbon fibers structure. In all cases, and for all studied pore widths a type-V adsorption isotherm (according to the IUPAC classification[34]) was observed. A stepwise condensation was found, with a hysteresis loop. This phenomenon was attributed to a capillary condensation-like transition. P. Monson and coworkers[32,33] have recently suggested that in porous carbons that are essentially free of active sites, the water vapour–liquid transition should take place above P_0 (*i.e.* the vapour branch of the hysteresis loop terminates above the bulk saturation conditions), while the equilibrium pressure between the two phases is presumably lower than P_0. This is consistent with the findings of Easton and Machin,[27] who measured water adsorption in graphitized carbon black and observed condensation in the supersaturated states of the bulk vapour.

If Monson's model holds true, the stable equilibrium state of water at saturation conditions corresponds to a carbon porous network filled with liquid, *even though the internal carbon surface is hydrophobic!* Classical capillary thermodynamics provides a simple explanation for this fact. In a sufficiently large pore of radius r_P the liquid–vapour equilibrium condition is described by Kelvin's equation[35]

$$\ln\left(\frac{P}{P_0}\right) = -\frac{2\gamma_{LV}\bar{V}_L\cos\theta}{RTr_P} \qquad (1)$$

where γ_{LV} is the liquid–vapour interfacial tension, $\bar{V}_L$ the liquid molar volume, r_P the pore radius and θ is the contact angle of the liquid on the solid surface. Such macroscopic laws are known to be valid even in the case of pores as small as 2–10 nm in size (the so-called mesoporous range).[36,37] We do not expect Kelvin's equation to be quantitatively valid in pores of radius <2 nm, because of specific confinement effects that may take place in such narrow pores,[29,33,38] and also because γ_{LV} and $\bar{V}_L$ will become pore size dependent and will not be equal to their bulk liquid values anymore.[39] Nevertheless, we believe that the Kelvin equation can still be used in a qualitative way to predict vapour–liquid condensation in micropores. The physical meaning, at the molecular level, of the interfacial tension γ_{LV} is associated with the potential energy needed to bring a molecule from the interior of a liquid to its surface. Its value (and the way it changes with the system size) is not easy to derive in nanoscopic systems, but the sign of this quantity will always be positive. Whether the vapour–liquid condensation will take place below, or above the saturation vapour pressure ($P/P_0 < 1$ or >1) will thus depend solely on the sign of $\cos\theta$. In a very interesting study, Werder *et al.*[28] have shown that the contact angle of water on graphite varies linearly with the water monomer binding energy on the graphite surface. This, in turn, can be directly linked with the Lennard-Jones ε_{CO} carbon–water potential parameter.[28] An examination of the molecular simulation studies performed on water–graphitic pore systems (see ref. 28), shows that the potential parameters mostly fall in the range corresponding to a contact angle of 60 to 85°. This is consistent, using eqn (1), with an equilibrium vapour–liquid transition taking place below P_0. On the experimental side, measured contact angle have been reported in the range of 42 to 86°.[40–42] A contact angle of roughly 85° is generally believed to be a reasonable value. It is interesting to note that a straightforward application of eqn (1) with $\theta = 85°$ and $r_P = 0.5$ nm, using the bulk liquid values for γ_{LV} and $\bar{V}_L$, yields to $P/P_0 = 0.83$, a value which compares quite well with the experimentally observed $P/P_0 \sim 0.8$ by Kaneko and co-workers in the case of microporous activated carbon fiber (P20 Ar).[24]

This brief (and inevitably incomplete) survey of the recent literature shows that a better understanding of water thermodynamics in hydrophobic solids was gained by studying water in porous carbons. Still, a more detailed understanding is hampered by the intrinsic disorder of the amorphous porous carbons (to our knowledge, no experimental equilibrium thermodynamics study of water in carbon nanotubes has appeared yet), as well as by the difficulty in obtaining samples free of active surface defects. Indeed, in many cases, Type-IV isotherms were observed,[19] which were interpreted as a combination of strong adsorption of a limited amount of water on primary adsorption sites ("hydrophilic" sites) at low pressure, followed by a plateau in the intermediate pressure range and finally a sudden filling of the nanoporous volume at a pressure below P_0. More recently, Rutherford confirmed the validity of the decomposition of a Type-IV isotherm into a combination of Type-I and Type-V isotherms.[43]

Other types of hydrophobic solids include mesoporous silica glasses[44] or micelle-templated silica,[36] in which the internal surfaces are grafted with alkyl chains of various lengths (usually organosilane molecules). In all these cases, a negligible water uptake is observed in the gas phase, and water can only enter the porous solid by applying a hydraulic pressure (forced intrusion) of a few tens of MPa,[45] a much larger value than the saturation vapour pressure $P_0 \cong 3500$ Pa. According to eqn (1), this means that the interface between water and the grafted silica is *non-wetting* (contact angle $> 90°$).

All-silica zeolites have also proven to behave like hydrophobic solids. In contrast to porous carbons and mesoporous silica, zeolites are well-characterized crystalline materials. The primary building unit of such solids is a tetrahedron with a silicon atom in the center and four oxygen atoms at its apexes. The zeolite framework consists of a 3-dimensional network of SiO_4 tetrahedra connected to each other by shared oxygen atoms. This enables to build up a variety of purely siliceous open framework materials containing cages and channels of

 This journal is © the Owner Societies 2008

0.4 to 2 nm width, with essentially no internal surface defects. In the all-silica frameworks such as silicalite-1[46] or beta zeolite,[47] water uptake in the gas phase at ambient conditions was found to be extremely small.[9] For this reason, these nanoporous materials were termed hydrophobic. In an experiment similar in nature to mercury porosimetry, Patarin and coworkers[48,49] observed water intrusion taking place in silicalite-1 at a hydraulic pressure of about 100 MPa at room temperature. A spontaneous extrusion (capillary evaporation, or drying) took place upon release of the pressure. Water intrusion above P_0 was also observed in the case of all-silica beta zeolite[48] and more recently in chabazite zeolite.[50,51] All-silica zeolites were thus proven to be highly *hydrophobic* as well as *non wetting* nanoporous materials.

At this stage it is important to point out the distinction between the concepts of hydrophobic surface, and of non-wetting interface. The first notion is based on the comparison between the surface–water and water–water interactions, and the second one is based on the contact angle value (*i.e.* on the interplay between 3 interface tension values, on account of the Young–Dupré equation). These two notions are of course related, in the sense that a non-wetting interface must correspond to a hydrophobic solid. However, the reverse is not true. A hydrophobic solid can exhibit a wetting solid–liquid interface. In such a case, the contact angle will be slightly less than 90°, as shown above in the case of porous carbons,[28,32,33] and water condensation will take place below P_0.

Recently, the water intrusion–extrusion transition in silicalite-1 was reproduced for the first time by equilibrium molecular simulations.[52,53] This phenomenon was tentatively interpreted in terms of an equilibrium first-order vapour–liquid condensation, following Porcheron *et al.*,[54] who pointed out the similarity between capillary condensation of a wetting fluid and forced intrusion of a non wetting fluid. However, no firm evidence was provided for the actual thermodynamic status of this transition. A sudden intrusion transition was also observed in the case of the all-silica form of chabazite.[50,51] However, in what follows we will show the recent results obtained in the case of ferrierite zeolite, in which water condensation seems to take place in a much more continuous way than in the other zeolites. Furthermore, water intrusion studied by different calorimetry methods was found to be exothermic in the case of amorphous mesoporous silica glasses,[44] while it was apparently endothermic in the case of silicalite-1.[45] It is one of our goal in this study to provide a clear thermodynamic understanding of this puzzling result.

In what follows, we report a new experimental water intrusion/extrusion study performed in the case of ferrierite zeolite, in which the fluid confinement is increased, as compared to silicalite-1, because of a smaller pore diameter. These results are compared with the previously published silicalite-1 data.[52,53] Monte Carlo simulations are then shown to be able to reproduce, at least qualitatively, the experimentally observed features. Finally, a thermodynamic analysis, based on the grand potential computation, leads us to propose a phase diagram of confined water in zeolites. Our conclusion is that the main features of the experimental intrusion/extrusion experiments can be understood in terms of equilibrium thermodynamics considerations.

The remainder of this article is organized as follows. The next section describes the synthesis and characterization of ferrierite zeolite, as well as the intrusion experiments. In section 3 we describe the models and methods used in the molecular simulation work. Section 4 deals with the experimental and simulation results for water adsorption in silicalite-1 and ferrierite. Last, section 5 gives a summary and conclusions.

2. Experimental

The ferrierite samples were synthesized according to the procedure published by Kuperman *et al.*,[55] in fluoride medium and using pyridine (py) and propylamine ($PrNH_2$) as structure-directing agent. The reaction gel had the following molar composition: 1,5-SiO_2 : 2 HF-py : 4 $PrNH_2$: 16 py : 8 H_2O. The reactants used were fumed silica (Aerosil 130), hydrogen fluoride–pyridine (70% (by weight) HF in pyridine, Aldrich), pyridine (SDS, 99.5%), propylamine (Fluka, 99%) and distilled water. After homogenization (slight stirring), the mixture was introduced in a Teflon-lined stainless-steel autoclave and heated at 180 °C during 5 days. After synthesis, the product was filtered, washed with distilled water and dried at 60 °C overnight. The solid was then calcined at 880 °C to completely remove the organic template. The as-synthesized and calcined products were characterized by X-ray diffraction (XRD), thermal analysis and solid state NMR spectroscopy.

The calcined ferrierite sample is very well crystallized (Fig. 1). Its XRD pattern was unambiguously indexed with an orthorhombic cell (space group *Pmnn*)[55] with a = 18 710(2), b = 14 060(2), c = 7415(1) Å. The elemental analysis of the calcined sample leads to the idealized unit cell formula $Si_{36}O_{72}$. The ^{29}Si MAS NMR spectrum reported in Fig. 2 displays 4 components in the −110 to −120 ppm range (reference TMS) ascribed to the 5 distinct crystallographic silicon sites and corresponding to Q4 groups ($Si–(OSi)_4$). No signal is observed at about −100 ppm corresponding to Q3 groups such as silanol groups revealing thus the absence of defect sites. Moreover, by thermogravimetric analysis, the amount of adsorbed water in the calcined sample at ambient conditions is approximately 1 wt% (*i.e.* 1 water molecules per

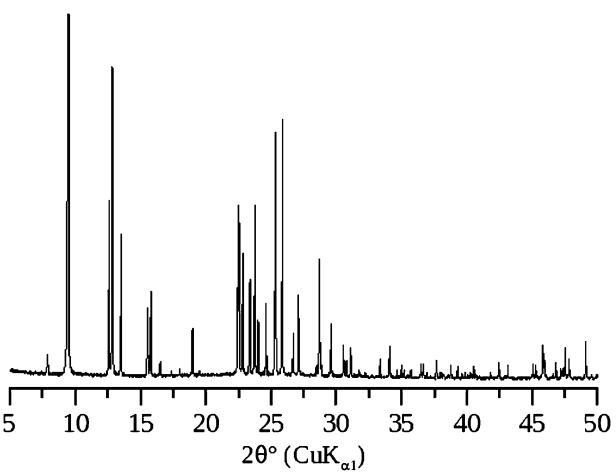

Fig. 1 XRD pattern of the calcined ferrierite sample (radiation Cu Kα1).

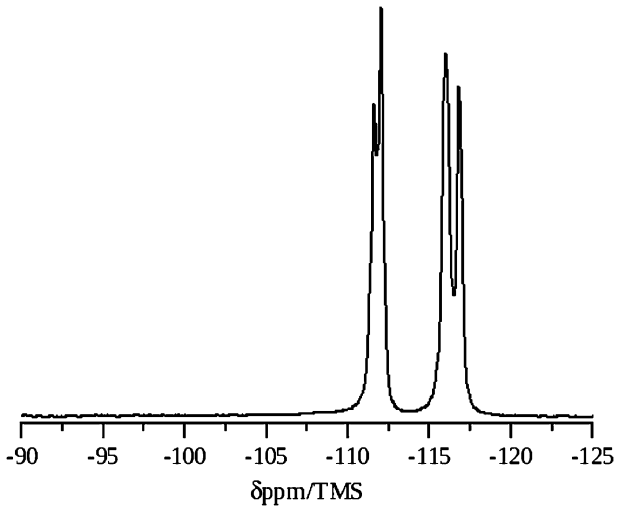

Fig. 2 ^{29}Si MAS NMR spectrum of the calcined ferrierite sample.

unit cell). Therefore, the ferrierite sample can be described as a strongly hydrophobic zeolite sample.

The intrusion-extrusion of water in the ferrierite samples was performed using a Micromeritics mercury porosimeter (Autopore IV model). The cell containing the water/zeolite system consists in a polypropylene cylinder of 2 cm^3 sealed by a mobile piston. This cell is introduced in the 15 cm^3 glass cell of the porosimeter which is filled with mercury. The volume variation is determined through a capacity measurement which depends on the mercury height in the capillary tube of the glass cell. The maximum volume change is about 0.2 cm^3. The experimental intrusion–extrusion curve is obtained after subtraction of the curve corresponding to the compressibility of pure water.

3. Molecular simulation models and methods

3.1 Silicalite-1 and ferrierite models and forcefields

Both zeolite frameworks consist of interconnected channels. The channel's diameter is ~5.4 Å in the case of silicalite-1. Ferrierite displays ellipsoidal channels (dimensions 4.1 × 5.4 Å). The fluid confinement is thus increased in the case of ferrierite, as compared to silicalite-1.

We used a rigid zeolite framework in both cases. We used for silicalite-1, the atomic coordinates of the orthorhombic (*Pnma*) structure determined by van Koningsveld *et al.*[56] (unit cell parameters: a = 20.022 Å; b = 19.899 Å and c = 13.383 Å), as explained in detail in a previous article.[9] In the case of ferrierite, we used the structural data reported above in the Experimental section. We simulated a box of eight unit cells in the case of silicalite-1 and twelve in the case of ferrierite, with periodic boundary conditions.

Molecular simulations were performed in the classical limit (no bond breaking taking place, for instance). This is justified by the fact that no structural or chemical changes seem to occur in silicalite-1 upon water condensation, even after several intrusion–extrusion cycles.[9] The forcefield used here was described in details earlier.[9,53,57] It has been used in previous water adsorption studies in either cationic[57] or all-silica frameworks.[9,53] The framework-fluid potential consists of standard Coulombic + Lennard-Jones terms that act between the zeolite and the water centres of forces. The TIP4P model was used for water. All the potential parameters used in this work are identical to those reported in ref. 9. Finally, Ewald sums were used to calculate the Coulombic terms of the interaction potential energy.

3.2 Simulation methods

Adsorption isotherms were computed using bias grand canonical Monte Carlo (GCMC) simulations[58–60] to compute the average number of adsorbed water molecules for several values of the chemical potential of the (fictitious) vapour reservoir at a given temperature. In the gas phase adsorption simulations, the water chemical potential was related to the vapour pressure by using the ideal gas law. Liquid phase adsorption data were obtained using the $\mu(P)$ relation, in a way previously described.[53] Other details such as the statistical bias moves, used to accelerate the convergence of the Monte Carlo runs, were also described in previous articles.[9,57] Each GCMC run lasted for some 10 million steps in order to equilibrate the system, followed by at least 40 million steps for the data acquisition.

3.3 Grand potential computation

The question of the nature of the transition in adsorption/desorption experiments is often subject to debate. Is this transition a real phase transition, between a gas-like and a liquid-like fluid? Likewise, when hysteresis occurs, its origin also raises several questions. Is it due to a bad sampling of the system or can it be related to the existence of multiple metastable states?[61] In order to provide an answer to these issues, knowledge of the thermodynamic potential of the system is necessary. Such a quantity is not straightforward to obtain and requires the use of sophisticated techniques. Recently, Wang and Landau developed such a technique based on the computation of the density of states (DOS) on-the-fly, using Monte Carlo simulations with non-Boltzmann sampling[62,63] (Once the DOS is known, the calculation of the thermodynamic potential is straightforward.) This method has been used successfully to study a wide range of systems, including Ising models,[64] Lennard-Jones fluids[65] and clusters,[66] or proteins.[65,66] It has also been revisited in the context of expanded ensembles.[67–70] In expanded ensembles, substates of the system are defined by the introduction of a new variable often called reaction coordinate ξ. The aim of those EXEDOS (expanded ensemble density of states) simulations is not to determine the density of states as a function of the energy, as in the original Wang–Landau algorithm, but as a function of the reaction coordinate, in order to compute variations of thermodynamic quantities along ξ. When dealing with adsorption, the thermodynamic potential is the grand potential Ω, since simulations are conducted in the grand canonical ensemble. We have applied the EXEDOS methodology to compute Ω as a function of the number of adsorbed water molecules in the zeolite framework. To this end, we have computed the density of states of the system as a function of N, denoted $Q(N)$.

 This journal is © the Owner Societies 2008

The probability to generate randomly a configuration with N water molecules is proportional to $Q(N)$. A flat distribution is thus obtained if each state is visited with probability proportional to $1/Q(N)$. The acceptance probabilities of insertion and destruction moves have been modified accordingly (rotations, translations, and jump moves are still accepted according to the conventional Metropolis criteria):

$$\mathrm{p}(N \rightarrow N+1) = \min\left(1, \frac{V}{(N+1)\Lambda^3}\frac{Q(N)}{Q(N+1)}\mathrm{e}^{-\beta\Delta E}\right) \quad (2)$$

$$\mathrm{p}(N \rightarrow N-1) = \min\left(1, \frac{N\Lambda^3}{V}\frac{Q(N)}{Q(N-1)}\mathrm{e}^{-\beta\Delta E}\right) \quad (3)$$

where Λ is the de Broglie wavelength and ΔE is the energy change between the new and the old configuration. The de Broglie wavelength value is irrelevant in classical simulations. It appears formally in these equations but its effect cancels out in the simulations.

$Q(N)$ is determined iteratively during the simulation. Initially, Q is uniformly set to 1 for the entire range of values accepted for N. Q is then updated at each insertion or destruction trial move between two configurations containing respectively N_1 and N_2 water molecules. If the move is accepted, $Q(N_2)$ is multiplied by a factor f (with $f > 1$); if the move is rejected, $Q(N_1)$ is multiplied by f. At the same time, a N-histogram $H(N)$ is accumulated. The simulation is stopped when each bin has been visited at least $100/\sqrt{\ln f}$ times, following Zhou and Batt.[70] At this time, the multiplicative factor is decreased, so that $f \rightarrow \sqrt{f}$. The histogram is reset to zero and a new cycle is started, until the histogram is flat again. This process is repeated until f reaches a small enough value. f is set to e^1 for the initial cycle, and 20 cycles are made, so that the last value of f is approximately equal to $\exp(10^{-6})$. For small values of f (typically $f < \exp(10^{-4})$), the "minimum visit per bin" criterion may be too restrictive and the simulation is stopped if the total number of MC moves is superior to $200\,000/\sqrt{\ln f}$, as suggested by Poulain *et al.*[65]

Once $Q(N)$, which corresponds to the canonical partition function, has been determined, one is able to compute Ω for the system, using:

$$\Omega(\mu, V, T) = -k_\mathrm{B}T\ln\left(\sum_N \mathrm{Q}(N)\mathrm{e}^{\beta\mu N}\right) \quad (4)$$

For a given value of the chemical potential μ, the Landau free energy Ω_L between two states containing, respectively, N_1 and N_2 molecules is:

$$\Omega_\mathrm{L}(\mu, N_2) - \Omega_\mathrm{L}(\mu, N_1) = -k_\mathrm{B}T\ln\left(\frac{Q(N_2)}{Q(N_1)}\mathrm{e}^{\beta\mu(N_2-N_1)}\right) \quad (5)$$

This allows to determine Ω_L to within an additive constant. In our particular case it turns out that $\Omega_\mathrm{L}(\mu, 0) = 0$ kJ mol^{-1}, since $N = 0$ corresponds to only one configuration for any value of μ. In what follows, we will be using the known $\mu(P)$ relationship for bulk water,[9] in order to compute Ω (or Ω_L) as a function of the external pressure of the reservoir.

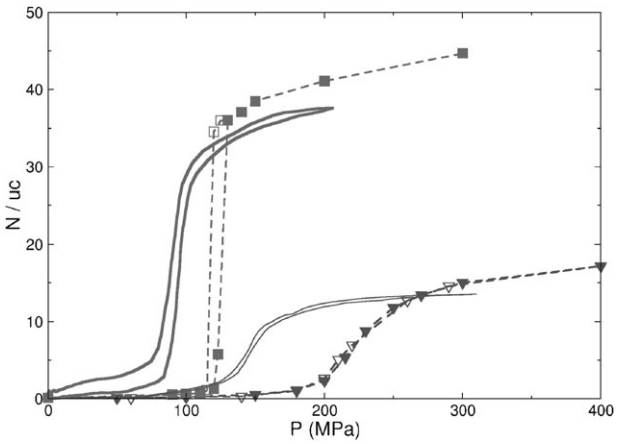

Fig. 3 Water intrusion/extrusion isotherms in silicalite-1 (squares and thick line) and ferrierite (triangles and thin line). Experimental data are shown in solid lines, symbols represent GCMC simulations (filled symbols: intrusion, open symbols: extrusion).

4. Results and discussion

4.1 Intrusion/extrusion experiments and equilibrium Monte Carlo simulations

In Fig. 3, we report the experimental intrusion–extrusion experiments in ferrierite, together with the results of the GCMC simulations. For comparison sake, we also report the previously published data obtained in the case of silicalite-1.[9]

The experimental intrusion and extrusion phenomenon in ferrierite was found to be reversible, within experimental uncertainties. This was also true in the simulations. The intrusion–extrusion phenomenon in the silicalite-1 has been studied earlier in some detail.[9,53] In both cases, the maximum water loading at high pressure is rather well reproduced by the simulations. As explained in details previously,[9] the water content at full loading is always a little bit smaller in the experiments than in the simulations, due to the existence of a small amount of preadsorbed water at ambient conditions in the porous samples ($\sim$1 to 2 wt%).

Water intrusion takes place at higher pressure in ferrerite than in silicalite. This could be expected on the basis of the simple argument of increased fluid confinement. In sufficiently wide pores the intrusion process can be described by the so-called Washburn equation:[71]

$$P = -\frac{2\gamma_\mathrm{LV}\cos\theta}{r_P} \quad (6)$$

where P is the hydraulic pressure that must be applied to the nonwetting liquid to penetrate a cylindrical pore of radius r_P. γ_LV and θ have the same meaning as in eqn (1). As already discussed in the Introduction, one does not expect that such a macroscopic equation to be valid for pore radius in the nanometer scale. The qualitative trend, however, should be valid: the intrusion pressure should increase with the fluid confinement, *i.e.* with a decreasing pore radius.

The pressure values at which the simulated condensation processes take place in these two zeolites are underestimated by 30 to 50%. However, this deviation corresponds to a 2–4%

difference in chemical potential only. This is due to the fact that $\left(\frac{\partial \mu}{\partial P}\right)_T$ is quite small in the liquid phase.[9,53] We note in passing that $\left(\frac{\partial \mu}{\partial P}\right)_T$, from a Maxwell relation, is the partial molar volume. Given the crudeness of the model (*e.g.* rigid framework), this result can be considered as satisfactory. It was demonstrated in earlier studies on water intrusion in silicalite-1, that small changes in the force field parameters could lead to a water condensation taking place in the gas phase instead of the liquid phase.[53,73,76] The intrusion pressure at room temperature was also shown to be extremely sensitive to small changes in the framework atomic coordinates.[57] The use of simple, non polarizable forcefields is questionable and is still debated in the literature.[72,73] It was shown for instance that the apparent dipole moment of the water molecule can be lowered by some 10 to 20% in LTA or silicalite-1, as compared to the apparent dipole moment in the bulk liquid phase.[73–75] Nevertheless, the simple model used in this work is able to qualitatively predict the water condensation phenomenon in both silicalite-1 and ferrierite all-silica zeolites without readjusting the potential parameters that we borrowed from previous gas phase adsorption studies.

The major new finding reported in Fig. 3 is that the GCMC simulations were able to qualitatively reproduce the large spreading of the water intrusion process in ferrierite (over some 100 MPa), while at the same time the intrusion phenomenon in silicalite-1 was much steeper. In what follows we examine in more details the nature of the condensation transition in both cases, in order to better understand the underlying physics that causes intrusion to be either an abrupt or a much more continuous process, depending on the extent of the fluid confinement.

4.2 Thermodynamic analysis of the intrusion transition

We report in Fig. 4 the Landau free energy Ω_L as a function of the number of intruded water molecules for various pressure, at 300 K. The water–silicalite-1 system (Fig. 4a), is characterized by the existence of a double potential well. Below 120 MPa, the most stable state corresponds to the empty zeolite, and the filled state is metastable. Above 120 MPa, the filled state has become the most stable one. The existence of two stable states is characteristic of a first-order transition between gas-like and liquid-like phases. The conversion between those two states is possible on a wide range of pressure as seen in Fig. 4a, but the system has to overcome a macroscopic energy barrier. Monte Carlo simulations proceed *via* microscopic moves. In a finite time Monte Carlo run, the most stable state may not be reached, and this is why a small hysteresis loop is observed.

In contrast, the water–ferrierite system (Fig. 4b) displays only one stable potential well. At 150 MPa the stable state is the empty zeolite. As pressure increases, the single stable state progressively moves along the N coordinate until the porous framework is completely filled ($\sim$400 MPa). This feature is reminiscent of a continuous phase transition, although there are other possible explanations. For instance the increased fluid confinement may lead to a pseudo 2D, or even 1D behaviour, for which it is known that the conventional views of the bulk phase transitions are no more valid.

A further insight is provided by the study of the intrusion phenomenon at various temperatures. In Fig. 5 a change in the shape of the isotherm as temperature is increased from 300 to 400 K, is clearly seen. From first-order, the transition becomes continuous-like. Note that the amount of adsorbed water is sketched against the chemical potential of the fluid reservoir, instead of its pressure. This is due to the fact that the $\mu(P)$ relationship for bulk water is only available at 300 K for the time being. In Fig. 6 we report the free energy for both zeolite-water systems at 3 different temperatures. Fig. 6a–c confirm that the first-order phase transition in silicalite-1 transforms into a continuous transition. Fig. 6d–f show that the continuous transition in ferrierite at 300 K (a single potential well), turns into a first-order transition (double well behaviour) as temperature is decreased to 200 K. The free energy profiles in Fig. 6(d) are a bit scattered, and this is due to a slower convergence of the EXEDOS algorithm as temperature is lowered. Another view of the same results is provided in Fig. 7, where the grand potential Ω is reported as a function of the chemical potential. In both zeolites a marked change in the slope of Ω is observed at low temperature (*i.e.* a first-order transition), which transforms into a continuous transition as temperature is increased.

The above results can clearly be interpreted in terms of the existence of a genuine first-order vapour–liquid transition line terminated by a critical point. A schematic phase diagram of confined water in zeolites is proposed in Fig. 8. In this tentative diagram, we concentrate on the vapour–liquid transition and the solid–liquid and solid–gas transitions are not

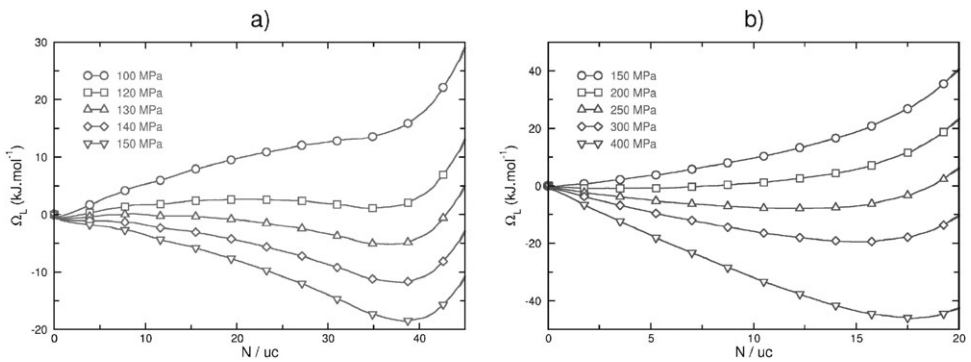

Fig. 4 Computed Landau free energy Ω_L of the water–zeolite system for various pressures at 300 K, as a function of the amount of intruded water. (a) silicalite-1, (b) ferrierite.

 This journal is © the Owner Societies 2008

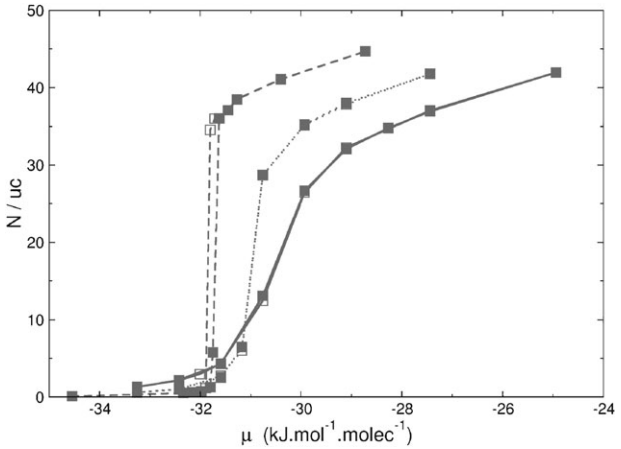

Fig. 5 Water intrusion/extrusion isotherms in silicalite-1 at 300 K (dashed line), 350 K (dotted line), and 400 K (solid line). Filled symbols are for intrusion and open symbols are for extrusion data.

considered in any details. This diagram is based on two simple assumptions related to fluid confinement in a hydrophobic solid: a shift of the vapour–liquid transition to higher pressure as confinement increases together with a shift of the critical point to lower temperature.[39] This provides a plausible qualitative explanation of the fact that, at 300 K, the vapour–liquid transition is first-order like in silicalite-1, while it turns into a smooth, supercritical, crossing from a diluted to a dense fluid in the case of ferrierite.

It might appear surprising that a bulk fluid phase diagram can be extended in such a way, down to the nanoscale range. Indeed, it is common wisdom, in the adsorption community, that the usual bulk phase transitions do not exist anymore in micropores,[34] and especially so in zeolites. Experimentalists in the adsorption community usually restrict the use of 'capillary condensation' to describe the filling of mesopores and macropores (*i.e.* in pores of widths $> \sim 2$ nm). Adsorption in microporous solids (pore widths < 2 nm) are usually characterized by reversible type-I isotherms. This view is valid for the adsorption of fluids that have a strong affinity with the adsorbent walls (it is typically the case in aluminosilicate zeolites). For large enough pores, surface wetting (or layering) occurs at low pressure, in undersaturated vapour. It is followed at higher vapour pressure by the fluid condensation in the pore interior. In their influential textbook on adsorption, Rouquerol, Rouquerol and Sing[34] describe capillary condensation as a "secondary process, which is always preceded by adsorption on the pore walls". What we learnt from the physics of phase transitions is that only for large pores can the surface and bulk effects be separated. An increasing mixture of surface and bulk transitions is known to take place as the pore narrows.[39,77] This explains why capillary condensation cannot be distinguished anymore from surface wetting in strongly-adsorbing microporous materials. The situation in which the fluid does not fully wet the pore surface is different. In this case, we believe that a first-order like condensation of the fluid can be observed, provided that the interconnected pore structure is 3-dimensional. In our first study of water condensation in silicalite-1, we observed that the transition occurred *everywhere* in the porous solid, at the same pressure. Even though each channel portion of the presently studied zeolites forms a pseudo 1D confined system, in which a first-order transition is theoretically forbidden, the interconnected nature of the porous structure and the correlation between adjacent pores[78] ensures a 3D-like behaviour of confined water. The occurrence of such a first order-like transition has actually been predicted by Bichara and Pellenq[79,80] in the case of selenium adsorption in silicalite-1 zeolite. A simulation of water confined to narrow carbon nanotubes has also revealed discontinuous as well as continuous solid–liquid phase changes.[81]

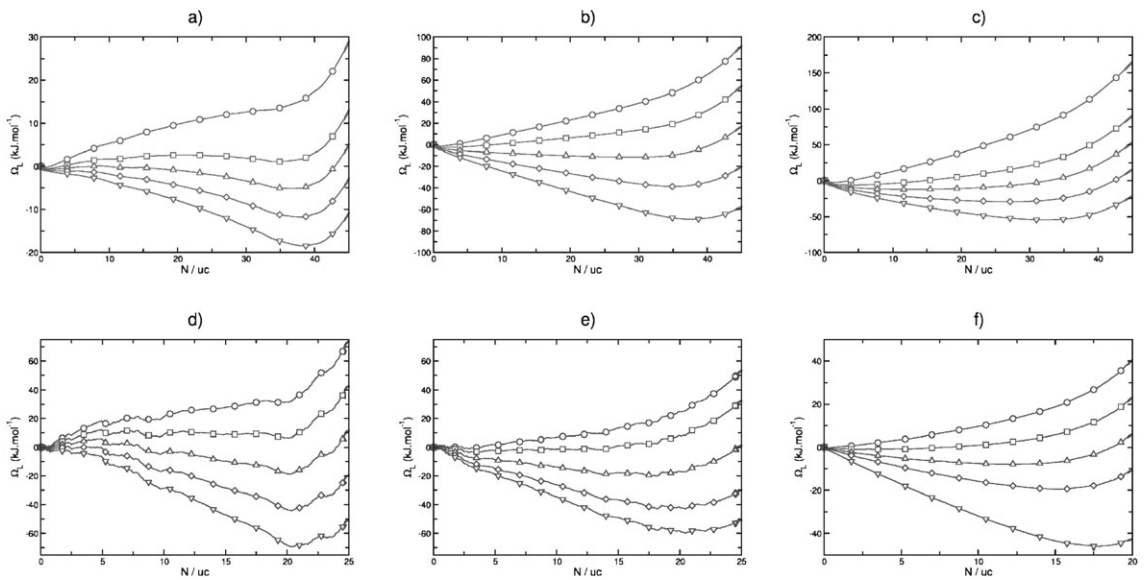

Fig. 6 Free energy profiles for various chemical potentials and temperatures for silicalite-1 (a, b, and c) and ferrierite (d, e, and f). (a) silicalite-1 at 300 K; (b) silicalite-1 at 350 K; (c) silicalite-1 at 400 K; (d) ferrierite at 200 K; (e) ferrierite at 230 K; (f) ferrierite at 300 K. In each graph, the chemical potential value (and thus the pressure) increases from the top profile to the bottom one.

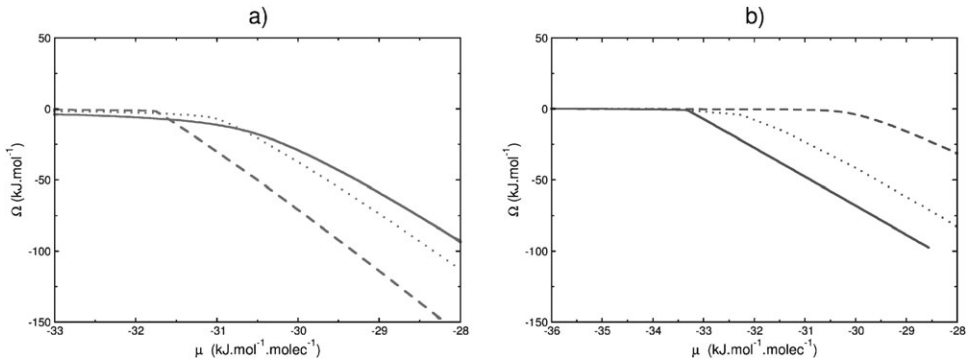

Fig. 7 Variation of the grand potential of the water–zeolite systems as a function of the chemical potential for various temperatures. (a) silicalite-1 at 300 K (dashed line), 350 K (dotted line), and 400 K (solid line); (b) ferrierite at 200 K (solid line), 230 K (dotted line), and 300 K (dashed line).

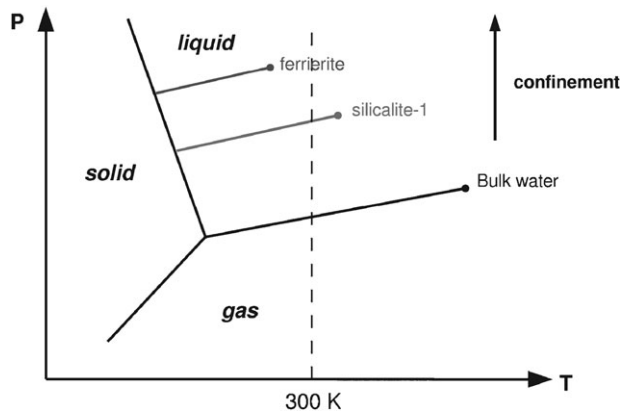

Fig. 8 Schematic phase diagram of confined water in zeolites.

This is to our knowledge the first time that the Wang–Landau algorithm is used in the context of fluid intrusion/extrusion in nanoporous solids, and that the existence of a genuine first-order transition is really demonstrated. We believe that this represents an important progress for the study of adsorption/intrusion processes, since we are now able to derive thermodynamic quantities that were not easily accessible until now.[82–84]

4.3 Heats of intrusion transition

As mentioned in the Introduction section, water intrusion studied by different calorimetry methods was found to be exothermic in the case of an amorphous mesoporous silica glasses,[44] while it was apparently endothermic in the case of silicalite-1.[45] This calls for a detailed examination of the heat effects during the intrusion transition. It must be reminded that the intrusion experiments involves *both* the zeolite sample and the bulk water reservoir. We shall concentrate here on the variation of the thermodynamic internal energy ΔU of the system at the intrusion transition, which is directly related, at the molecular level, to the variation in the water potential energy ΔE_p. The total potential energy of a system made of N water molecules in the bulk reservoir and N^Z molecules confined in the zeolite solid is:

$$E_p = E_{water}^{zeolite} + E_{water}^{bulk} = N^Z\overline{E^Z} + (N - N^Z)\overline{E^b} \qquad (7)$$

Where $\overline{E^i}$ is the potential energy per molecule in the zeolite (i = Z) or in the bulk fluid (i = b). The first-order intrusion transition (constant T and P), takes place between an initial state 1, in which the zeolite is filled with water vapour (N_1^Z) and surrounded by bulk liquid, and the final state 2 in which $N_2{}^Z$ molecules in the liquid state have been transferred from the bulk to the interior of the zeolite. The change in potential energy of the system writes:

$$\begin{aligned}\Delta E_p &= E_{p,2} - E_{p,1} \\ &= N_2^Z\overline{E_2^Z} - N_1^Z\overline{E_1^Z} + [N(\overline{E_2^b} - \overline{E_1^b}) + N_1^Z\overline{E_1^b} - N_2^Z\overline{E_2^b}]\end{aligned} \qquad (8)$$

given that $\overline{E_1^b} = \overline{E_2^b} = \overline{E^b}$, this equation can be rewritten as:

$$\Delta E_p = N_2^Z\overline{E_2^Z} - N_1^Z\overline{E_1^Z} + \overline{E^b}(N_1^Z - N_2^Z) \qquad (9)$$

or equivalently:

$$\Delta E_p = N_1^Z(\overline{E^b} - \overline{E_1^Z}) + N_2^Z(\overline{E_2^Z} - \overline{E^b}) \qquad (10)$$

Since the internal zeolite surface is hydrophobic, $\overline{E^b} < \overline{E_1^Z}$ and $\overline{E^b} \leq \overline{E_2^Z}$. The first term of eqn (10) is thus negative and the second one positive. The overall sign of ΔE_p results from a balance between these two terms of opposite signs.

In the limiting case of large enough pores, so that the surface effects are negligible ($\overline{E_1^Z} = 0$; $\overline{E_2^Z} = \overline{E^b} = -41.8$ kJmol^{--1}), the heat effect is dominated by the first (negative) term. This corresponds to a simple vapour condensation in an unconfined system, which is naturally exothermic. In the second limiting case of very small pores, for which $\overline{E_2^Z} \gg \overline{E^b}$ (the water–surface interactions in the confined fluid are dominant with respect to the water–water interactions), the heat effect is dominated by the second (positive) term, and the overall intrusion process becomes endothermic. This provides an explanation for the observed experimental calorimetric features mentioned above. In this model, we only take the thermodynamic internal energy into account. The measured transition heat effects correspond to an enthalpy change, and we thus neglect the $P\Delta V$ term. This term is always negative for the intrusion transition, and only a change in the sign of the internal energy can explain the change from an endothermic to an exothermic effect.

In order to compare our calculations with the heat flow experiments, we report in Fig. 9 the derivative of E_p, computed

 This journal is © the Owner Societies 2008

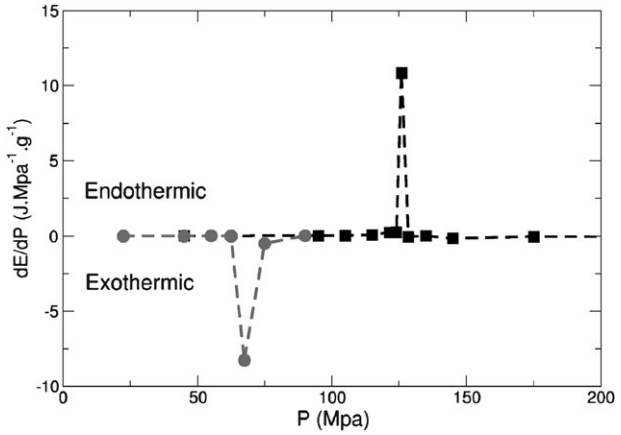

Fig. 9 Derivative of internal energy of the zeolite–water system against pressure in the case of silicalite-1 (squares) and faujasite (circles). Dashed lines are guides to the eye.

using the above model, in the case of silicalite-1. The results compare quite well with the published data of Coiffard *et al.* (ref. 45, Fig. 3c). We have also examined the case of a hypothetical all-silica faujasite (which is a large cage zeolite) and found that the intrusion would be endothermic in this latter case. As already mentioned by Coiffard *et al.*,[45] it would seem possible to find a nanoporous solid that has the right pore diameter, in order for the intrusion/extrusion process to become athermal. One would then be able to device, along these lines, a mechanical energy storage (and release) system that works without heat effects.

We conclude that the change in the sign of the heats of intrusion can simply be understood in terms of equilibrium thermodynamics consideration, in contrast with the liquid flow irreversibility arguments that were suggested earlier.[45]

5. Summary and conclusions

The behaviour of water in nanoporous hydrophobic solids was mostly studied up to now in the special (and important) case of porous carbon materials. All-silica zeolites are well characterized solids and can be prepared with almost no internal surface defects.[9] A combination of experiments and molecular simulations, using such materials, enabled us to shed some new light on the water condensation process that takes place in hydrophobic solids.

The main conclusion of this study is that water condensation takes place through a genuine first-order phase transition, provided that the interconnected pores structure is 3-dimensional. In extreme confinement situations (such as in ferrierite zeolite), condensation may take place through a continuous supercritical crossing from a diluted to a dense fluid, on account of the fact that the first-order transition line is shifted to higher pressure, and the confined water critical point is correlatively shifted to lower temperature. This is at odds with the common belief that conventional phase transitions cannot take place in microporous solids such as zeolites.

We believe that this finding is very general for hydrophobic solids, *i.e.* for both nonwetting as well as wetting water–solid interface systems (the condensation transition being an *intrusion* transition in the first case and a classical *capillary condensation* in the second one). In the case of the raw porous carbon materials, the first-order capillary condensation transition is presumably masked by the effects of pore size distribution (PSD) and surface defects.[23] When studying activated carbon fibers materials displaying narrow PSD and a low amount of surface defects, Kaneko and co-workers clearly showed that water condensation became quite steep.[24] This is consistent with the Monson model of water condensation in porous carbons.[32,33]

In the intrusion experiments, a rather high hydraulic pressure must be applied until the sudden fluid penetration takes place. This has lead to several interpretations of this phenomenon in terms of irreversibilities,[44,45,48,49] especially since hysteresis was often observed in standard experiments such as mercury intrusion.[54] Only recently has this process been examined in the light of equilibrium statistical thermodynamics.[85] The similarity between capillary condensation of a wetting fluid and forced intrusion of a non wetting fluid was, for a long time, overlooked.[54]

What we show here is that the most important features of the intrusion/extrusion process can be understood in terms of equilibrium thermodynamics considerations. Water intrusion is a first order vapour–liquid transition that takes place above the saturation vapour pressure because the water–solid interface in non-wetting. The accompanied heat effect is either endo- or exothermic, depending on the pore size of the hydrophobic materials, and this can be accounted for by considering the changes in internal energy of water inside as well as outside the porous solid.

Acknowledgements

This work was supported by the French "Agence Nationale de la Recherche", under contract # BLAN06-3_144027. The authors wish to acknowledge Roland Pellenq for fruitful discussions and for providing them with the results of ref. 73 prior to publication.

References

1. F. H. Stillinger, *J. Solution Chem.*, 1973, **2**, 141.
2. A. Wallqvist and B. Berne, *J. Phys. Chem.*, 1995, **99**, 2893.
3. Y. Cheng and P. Rossky, *Nature*, 1998, **392**, 696.
4. K. Lum, D. Chandler and J. D. Weeks, *J. Phys. Chem. B*, 1999, **103**, 4570.
5. T. Koishi, S. Yoo, K. Yasuoka, X. C. Zeng, T. Narumi, R. Susukita, A. Kawai, H. Frusawa, A. Suenega, N. Okitmoto, N. Futasugi and T. Ebisuzaki, *Phys. Rev. Lett.*, 2004, **93**, 185701.
6. P. Ball, *Chem. Rev.*, 2008, **108**, 74.
7. S. Rajamani, T. M. Truskett and S. Garde, *Proc. Natl. Acad. Sci. U. S. A.*, 2005, **102**, 9475.
8. N. Giovambattista, P. G. Debenedetti and P. J. Rossky, *J. Phys. Chem. C*, 2007, **111**, 1323.
9. M. Trzpit, M. Soulard, J. Patarin, N. Desbiens, F. Cailliez, A. Boutin, I. Demachy and A. H. Fuchs, *Langmuir*, 2007, **23**, 10131.
10. F. Cailliez, G. Stirnemann, I. Demachy, A. Boutin and A. H. Fuchs, *J. Phys. Chem. C*, 2008 DOI: 10.1021/jp710746b.
11. P. Ball, *Nature*, 2003, **423**, 25.
12. D. Chandler, *Nature*, 2002, **417**, 491.
13. J. Stelzer, M. Paulus, M. Hunger and J. Weitkamp, *Microporous Mesoporous Mater.*, 1998, **22**, 1.

14. R. N. Eissmann and M. D. LeVan, *Ind. Eng. Chem. Res.*, 1993, **32**, 2752.
15. M. Wikström, *Curr. Opin. Struct. Biol.*, 1998, **8**, 480.
16. O. Beckstein and M. S. P. Sansom, *Proc. Natl. Acad. Sci. U. S. A.*, 2003, **100**, 7063.
17. M. D. Collins, G. Hummer, M. L. Quillin, B. W. Matthews and S. M. Gruner, *Proc. Natl. Acad. Sci. U. S. A.*, 2005, **102**, 16668.
18. B. Pereira, S. Jain and S. Garde, *J. Chem. Phys.*, 2006, **124**, 074704.
19. J. K. Brennan, T. J. Bandosz, K. T. Thompson and K. E. Gubbins, *Colloids Surf., A*, 2001, **187–188**, 539.
20. M. M. Dubinin, *Carbon*, 1980, **18**, 355; M. M. Dubinin, *Carbon*, 1981, **19**, 402.
21. S. J. Gregg and S. K. W. Sing, *Adsorption, Surface Area and Porosity*, Academic Press, London, 2nd edn, 1982.
22. F. Rodriguez-Reinoso, M. Molina-Sabio and M. T. Gonzalez, *Langmuir*, 1997, **13**, 2354.
23. J. Alcaniz-Monge, A. Linares-Solano and B. Rand, *J. Phys. Chem. B*, 2002, **106**, 3209.
24. T. Kimura, H. Kanoh, T. Kanda, T. Ohkubo, Y. Hattori, Y. Higaonna, R. Denoyel and K. Kaneko, *J. Phys. Chem. B*, 2004, **108**, 14043.
25. M. M. Dubinin and V. V. Serpinsky, *Carbon*, 1981, **19**, 402.
26. T. Ohba, H. Kanoh and K. Kaneko, *J. Am. Chem. Soc.*, 2004, **126**, 1560; T. Ohba, H. Kanoh and K. Kaneko, *NanoLett.*, 2005, **5**, 227; T. Ohba, H. Kanoh and K. Kaneko, *Chem.–Eur. J.*, 2005, **11**, 4890.
27. E. B. Easton and W. D. Machin, *J. Colloid Interface Sci.*, 2000, **231**, 204.
28. T. Werder, J. H. Walther, R. L. Jaffe, T. Halicioglu and P. Koumoutsakos, *J. Phys. Chem. B*, 2003, **107**, 1345.
29. A. Striolo, A. A. Chialvo, P. T. Cummings and K. E. Gubbins, *Langmuir*, 2003, **19**, 8583.
30. T. Ohba, H. Kanoh and K. Kaneko, *J. Phys. Chem. B*, 2004, **108**, 14964.
31. A. M. Slasi, M. Jorge, F. Stoeckli and N. A. Seaton, *Carbon*, 2003, **41**, 479.
32. J.-C. Lui and P. A. Monson, *Langmuir*, 2005, **21**, 10219.
33. J.-C. Lui, P. A. Monson and F. van Swol, *J. Phys. Chem. C*, 2007, **111**, 15976.
34. F. Rouquerol, J. Rouquerol and K. Sing, *Adsorption by Powders and Porous Solids*, Academic Press, 1999, p. 442.
35. W. Thomson, *Proc. R. Soc. Edinburgh*, 1870, **7**, 63; W. Thomson, *Proc. R. Soc. Edinburgh*, 1871, **42**, 448.
36. B. Lefevre, A. Saugey, J.-L. Barrat, L. Bocquet, E. Charlaix, P. F. Gobin and G. Vigier, *J. Chem. Phys.*, 2004, **120**, 4927.
37. L. R. Fischer, R. A. Gamble and J. Middlehurst, *Nature*, 1981, **290**, 575.
38. P. Bordarier, M. Schoen and A. H. Fuchs, *Phys. Rev. E*, 1998, **57**, 1621.
39. I. Brovchenko, A. Geiger and A. Oleinikova, *J. Chem. Phys.*, 2004, **120**, 1958.
40. F. M. Fowkes and W. D. Harkins, *J. Am. Chem. Soc.*, 1940, **62**, 3377.
41. M. E. M. Tadros, P. Hu and A. W. Adamson, *J. Colloid Interface Sci.*, 1974, **49**, 184.
42. M. E. Schrader, *J. Phys. Chem.*, 1980, **84**, 2774.
43. S. W. Rutherford, *Langmuir*, 2006, **22**, 9967.
44. F. Gomez, R. Denoyel and J. Rouquerol, *Langmuir*, 2000, **16**, 4374.
45. L. Coiffard, V. A. Eroshenko and J.-P. Grolier, *AIChE J.*, 2005, **51**, 1246.
46. E. M. Flanigen, J. M. Bennet, R. W. Grose, J. P. Cohen, R. L. Patton, R. Kirshner and J. V. Smith, *Nature*, 1978, **271**, 512.
47. M. A. Camblor, A. Corma and S. Valencia, *Chem. Commun.*, 1996, 2365.
48. V. Eroshenko, R.-C. Regis, M. Soulard and J. Patarin, *J. Am. Chem. Soc.*, 2001, **123**, 8129.
49. V. Eroshenko, R.-C. Regis, M. Soulard and J. Patarin, *C. R. Phys.*, 2002, **3**, 111.
50. M. Trzpit, M. Soulard and J. Patarin, *Chem. Lett.*, 2007, **36**, 980–981.
51. M. Trzpit, S. Rigolet, J. L. Paillaud, C. Marichal, M. Soulard and J. Patarin, *J. Phys. Chem. B*, 2008, **112**, 7257.
52. N. Desbiens, I. Demachy, A. H. Fuchs, H. Kirsch-Rodeschini, M. Soulard and J. Patarin, *Angew. Chem., Int. Ed.*, 2005, **44**, 5310–5313.
53. N. Desbiens, A. Boutin and I. Demachy, *J. Phys. Chem. B*, 2005, **109**, 24071.
54. F. Porcheron, P. A. Monson and M. Thommes, *Langmuir*, 2004, **20**, 6482.
55. A. Kuperman, S. Nadimi, S. Oliver, G. A. Ozin, J. M. Garces and M. M. Olken, *Nature*, 1993, **365**, 239.
56. H. van Koningsveld, J. C. Hansen and H. van Bekkum, *Zeolites*, 1990, **10**, 235.
57. A. Di Lella, N. Desbiens, A. Boutin, I. Demachy, P. Ungerer, J.-P. Bellat and A. H. Fuchs, *Phys. Chem. Chem. Phys.*, 2006, **8**, 5396.
58. D. Nicholson and N. Parsonage, *Computer Simulation and the Statistical Mechanics of Adsorption*, Academic Press, New York, 1982.
59. A. H. Fuchs and A. K. Cheetham, *J. Phys. Chem. B*, 2001, **105**, 7375.
60. D. Frenkel and B. Smit, *Understanding Molecular Simulations. From Algorithms to Applications*, Academic Press, London, 2nd edn, 2002.
61. H. J. Woo and P. A. Monson, *Phys. Rev. E: Stat., Nonlinear, Soft Matter Phys.*, 2003, **67**, 041207.
62. F. Wang and D. Landau, *Phys. Rev. E: Stat., Nonlinear, Soft Matter Phys.*, 2001, **64**, 056101.
63. F. Wang and D. Landau, *Phys. Rev. Lett.*, 2001, **86**, 2050.
64. M. Shell, P. Debenedetti and A. Panagiotopoulos, *Phys. Rev. E: Stat., Nonlinear, Soft Matter Phys.*, 2002, **66**, 056703.
65. P. Poulain, F. Calvo, R. Antoine, M. Broyer and P. Dugourd, *Phys. Rev. E: Stat., Nonlinear, Soft Matter Phys.*, 2006, **73**, 056704.
66. N. Rathore and J. de Pablo, *Abstr. Pap. Am. Chem. Soc.*, 2002, **224**, U485.
67. E. Kim, R. Faller, Q. Yan, N. Abbott and J. de Pablo, *J. Chem. Phys.*, 2002, **117**, 7781.
68. N. Rathore, Q. Yan and J. de Pablo, *J. Chem. Phys.*, 2004, **120**, 5781.
69. M. Chopra, M. Müller and J. de Pablo, *J. Chem. Phys.*, 2006, **124**, 134102.
70. C. Zhou and R. Bhatt, *Phys. Rev. E: Stat., Nonlinear, Soft Matter Phys.*, 2005, **72**, 025701.
71. E. W. Washburn, *Phys. Rev.*, 1921, **17**, 273.
72. D. Bougeard and K. S. Smirnov, *Phys. Chem. Chem. Phys.*, 2007, **9**, 226.
73. J. Puibasset and R. J. M. Pellenq, *J. Phys. Chem. B*, 2008, in press.
74. K. S. Smirnov and D. Bougeard, *Chem. Phys.*, 2003, **292**, 53.
75. F.-X. Coudert, R. Vuilleumier and A. Boutin, *ChemPhysChem*, 2006, **7**, 2464.
76. C. E. Ramachandran, S. Chempath, L. J. Broadbelt and R. Q. Snurr, *Microporous Mesoporous Mater.*, 2006, **90**, 293.
77. S. Sacquin, M. Schoen and A. H. Fuchs, *J. Chem. Phys.*, 2003, **118**, 1453.
78. R. Radhakrishnan and K. E. Gubbins, *Phys. Rev. Lett.*, 1997, **79**, 2847.
79. C. Bichara, J. Y. Raty and R. J. M. Pellenq, *Phys.Rev. Lett.*, 2002, **89**, 016101-1.
80. C. Bichara, J. Y. Raty and R. J. M. Pellenq, *Mol. Simul.*, 2004, **30**, 601.
81. K. Koga, G. T. Gao, H. Tanaka and X. C. Zeng, *Physica A*, 2002, **314**, 462.
82. B. K. Peterson and K. E. Gubbins, *Mol. Phys.*, 1987, **62**, 215.
83. J. Puibasset and R. J. M. Pellenq, *J. Chem. Phys.*, 2005, **122**, 094704.
84. M. Jeffroy, A. H. Fuchs and A. Boutin, *Chem. Commun.*, 2008, 28, DOI: 10.1039/b805117h.
85. F. Porcheron, M. Thommes, R. Ahmad and P. A. Monson, *Langmuir*, 2007, **23**, 3372.

This journal is © the Owner Societies 2008

View publication stats